

Light coupling structures and switches for plasmonic coaxial waveguides

Cite as: J. Appl. Phys. **129**, 193103 (2021); <https://doi.org/10.1063/5.0043936>

Submitted: 12 January 2021 . Accepted: 06 May 2021 . Published Online: 21 May 2021

 Amirreza Mahigir, and  Georgios Veronis



View Online



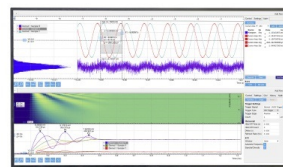
Export Citation



CrossMark

Challenge us.

What are your needs for periodic signal detection?



Zurich
Instruments



Light coupling structures and switches for plasmonic coaxial waveguides

Cite as: J. Appl. Phys. **129**, 193103 (2021); doi: [10.1063/5.0043936](https://doi.org/10.1063/5.0043936)

Submitted: 12 January 2021 · Accepted: 6 May 2021 ·

Published Online: 21 May 2021



View Online



Export Citation



CrossMark

Amirreza Mahigir^{1,2}  and Georgios Veronis^{1,2,a)} 

AFFILIATIONS

¹School of Electrical Engineering and Computer Science, Louisiana State University, Baton Rouge, Louisiana 70803, USA

²Center for Computation and Technology, Louisiana State University, Baton Rouge, Louisiana 70803, USA

Note: This paper is part of the Special Topic on Plasmonics: Enabling Functionalities with Novel Materials.

a) Author to whom correspondence should be addressed: gveronis@lsu.edu

ABSTRACT

We introduce wavelength-scale light coupling structures and switches for plasmonic coaxial waveguides. We first consider single-slit structures optimized for a wavelength of 1550 nm and find that, when the slit is on resonance, the coupling to the plasmonic coaxial waveguide is maximized. We also observe that for optimized double- and triple-slit structures, the coupling efficiency is enhanced compared to the single-slit structure by factors of ~ 3.02 and ~ 4.21 , respectively. We find that, in the case of double- and triple-slit structures, the surface plasmons excited at the metal–air interface enhance light coupling to the plasmonic coaxial waveguide via the slits. In addition, we investigate slit-based outcoupling structures for light extraction from the waveguide into a free space. We observe that while the far-field radiation pattern of single-slit structures is symmetric, double- and triple-slit structures have asymmetric radiation patterns. We also show that by exciting the incoupling slit structures at proper angles, we can excite only the right- or the left-propagating mode of the plasmonic coaxial waveguide. We finally design compact plasmonic switches consisting of a plasmonic coaxial waveguide side-coupled to a periodic array of two open-circuited coaxial stub resonators. Such a structure is based on a plasmonic analog of electromagnetically induced transparency and supports a slow-light mode. The space between the metallic parts is filled with an active material with a tunable refractive index. We show that the modulation depth of this structure is large enough for optical switching applications.

Published under an exclusive license by AIP Publishing. <https://doi.org/10.1063/5.0043936>

I. INTRODUCTION

Plasmonic waveguides are important components of integrated photonic circuits due to their ability to guide light with subwavelength optical modes.^{1–17} A variety of nanoplasmonic waveguides have been investigated.^{11,18–25} In particular, metal–dielectric–metal (MDM) plasmonic waveguides have attracted a lot of attention, owing to their broad spectral range of operation.^{26,27} Since there is no cutoff frequency for the fundamental mode of MDM waveguides, they are able to support deep subwavelength modes. This feature enables MDM waveguides to squeeze optical modes to nanoscale volumes, which are suitable for realizing nanophotonic devices.²⁸

Plasmonic coaxial waveguides, which are based on an MDM configuration, have been investigated both theoretically and experimentally in the past several years.^{29–35} It has been shown that sharp 90° bends and T-splitters based on plasmonic coaxial waveguides can be implemented with nearly no bending loss other than

the inherent ohmic loss of the straight waveguide itself over a broad wavelength range, including the optical communication wavelength of 1550 nm.³¹

Developing coupling nanostructures in order to efficiently excite the fundamental mode of plasmonic waveguides, when they are illuminated by a free-space radiation source, is important for applications of plasmonics.^{36,37} Several different coupling structures for quasi-two-dimensional MDM waveguides have been investigated both theoretically and experimentally.^{36,38–42} It has been shown that compact wavelength-scale slit-based structures can efficiently couple free-space light into quasi-two-dimensional subwavelength MDM plasmonic waveguides.^{37,43–46} Developing active plasmonic devices such as switches and modulators is another important challenge for on-chip applications of plasmonics.^{47,48}

In this paper, we introduce wavelength-scale light coupling structures and switches for plasmonic coaxial waveguides. We first consider a single-slit coupling structure and show that, by optimizing

the slit dimensions at the wavelength of 1550 nm, we can maximize the coupling efficiency to the plasmonic coaxial waveguide. We also show that the coupling efficiency exhibits maxima when a Fabry–Pérot resonance condition is satisfied. We then consider double- and triple-slit coupling structures. We show that for such structures, the light power coupled into the slits is greatly enhanced. The optimized double- and triple-slit structures result in ~ 3.02 and ~ 4.21 times coupling enhancement, respectively, compared to the optimized single-slit structure. In addition, we investigate the outcoupling efficiency of the proposed slit-based structures for extraction of light from the plasmonic coaxial waveguide to the free space. We show that slit-based couplers, functioning as slit nanoantennas, efficiently couple the fundamental mode of the plasmonic coaxial waveguide to free-space radiation, which can be collected at a light detector located in the far-field region of the slit nanoantennas. We also show that, while for a single-slit nanoantenna the radiation pattern is symmetric, for double- and triple-slit structures, the radiation pattern is asymmetric and the direction of maximum radiation can be tuned through the design parameters of the coupling structure. In addition, we show that, by exciting the incoupling slit structures at proper angles, we can excite only the right- or the left-propagating mode of the plasmonic coaxial waveguide. We finally design compact plasmonic switches consisting of a plasmonic coaxial waveguide

side-coupled to a periodic array of two open-circuited coaxial stub resonators.

The remainder of the paper is organized as follows. In Sec. II, we first define the transmission cross section of the plasmonic coaxial waveguide for a given coupling structure and briefly describe the simulation method used for the analysis of the couplers. In Subsections II A–II C, we investigate single-, double-, and triple-slit incoupling structures, respectively. In Subsection II D, we investigate outcoupling structures as well as the asymmetric excitation of the modes of the plasmonic coaxial waveguide. In Subsection II E, we design compact switches for plasmonic coaxial waveguides. Finally, in Sec. III, we summarize our conclusions.

II. RESULTS

Nanostructures for efficiently coupling free-space light into plasmonic coaxial waveguides have not been previously investigated. In Subsections II A–II C, we investigate slit-based nanostructures through which the fundamental mode of plasmonic coaxial waveguides is excited by normally incident free-space waves. The cross section of the reference plasmonic coaxial waveguide investigated in this paper is shown in Fig. 1(d). The waveguide is placed on top of a silicon (Si) substrate, and the space between the inner

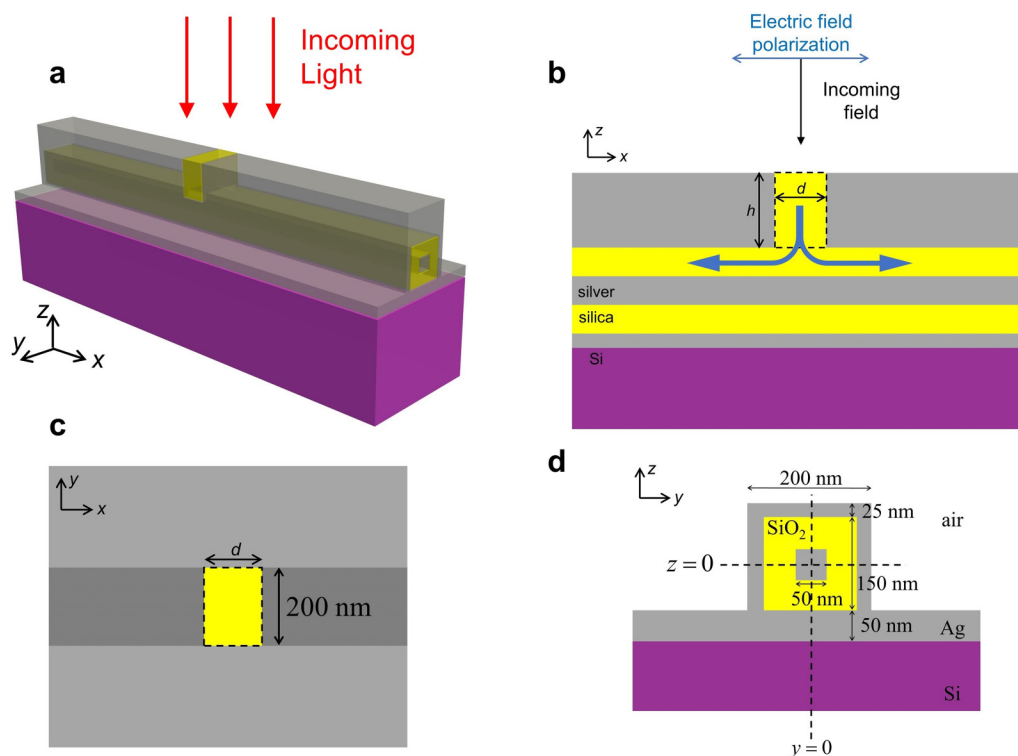


FIG. 1. (a) Schematic of the proposed nanostructure for exciting the fundamental guided mode of the plasmonic coaxial waveguide. The normally incident plane wave excites the guided modes of the slit that in turn excite the modes of the plasmonic coaxial waveguide. (b) Cross-sectional view of the coupler structure at the $y = 0$ plane. (c) Cross-sectional view of the coupler structure at the interface between the slit and air. (d) Cross section of the reference plasmonic coaxial waveguide. Silver is used as the metal and silica as the dielectric.

and outer coaxial metals is filled with silica (SiO_2). The metal used here is silver (Ag). We introduce coupling slits in the upper metallic side of the waveguide [Fig. 1(a)].

For a normally incident plane wave on a symmetric coupling structure, the power coupled into the plasmonic coaxial waveguide is equally divided between the modes propagating in the left and right direction. To quantify the coupling efficiency of a slit structure, we define its transmission cross section σ_T as the ratio of the amount of optical power that is coupled to the fundamental quasi-TEM mode of the waveguide propagating in the right direction over the incoming free-space optical power density.³⁷

We use the three-dimensional finite-difference time-domain (FDTD) method to numerically calculate the transmission in the plasmonic coaxial waveguide (Lumerical FDTD Solutions).⁴⁹ Dielectric permittivity data for silver and silica are obtained from CRC and Palik, respectively.^{50,51} We use the perfectly matched layer (PML) absorbing boundary condition on all sides of the simulation domain.⁵² We use a nonuniform simulation grid with grid size as small as 1 nm inside the waveguide and the slit regions and as large as 20 nm away from the waveguide. An incident plane wave excites the structure.

A. Single-slit coupler

We start by investigating a single-slit structure as a coupler between free-space light and the fundamental mode of the plasmonic coaxial waveguide [Figs. 1(a)–1(c)]. The dielectric core area of the waveguide is $A = 2 \times 10^4 \text{ nm}^2$ [Fig. 1(d)]. In Fig. 2(a), we vary the width d and the length h of the slit and calculate its transmission cross section σ_T (in units of A). The maximum coupling

efficiency is achieved when $d = 70 \text{ nm}$ and $h = 95 \text{ nm}$ with $\sigma_T \sim 4.9 A$.

We use the scattering matrix theory to model the coupling mechanism.³⁷ We calculate the transmission (t_i) and reflection (r_i) coefficients defined in Fig. 3 using FDTD. We also use FDTD to calculate the transmission cross section σ_{T_i} of the silver–silica–silver MDM slit [Fig. 3(a)]. Using scattering matrix theory, we find that the transmission cross section σ_T of the single-slit coupler [Fig. 1(a)] is given by³⁷

$$\sigma_T = \sigma_{T_i} \eta_{\text{res}_1} T_{\text{splitter}}, \quad (1)$$

where $T_{\text{splitter}} = |t_1|^2$ is the power transmission coefficient of the waveguide junction of Fig. 3(b), $\eta_{\text{res}_1} = \left| \frac{\exp(-\gamma_1 h)}{1 - r_1 r_2 \exp(-2\gamma_1 h)} \right|^2$ is the resonance enhancement factor of the silver–silica–silver MDM slit resonator, and $\gamma_1 = \alpha_1 + i\beta_1$ is the complex wavenumber of the fundamental propagating quasi-TEM mode in the silver–silica–silver MDM slit. We observe that, when $\arg(r_1) + \arg(r_2) - 2\beta_1 h = -2m\pi$ (for integer m), the slit is on resonance and η_{res_1} is maximized. In other words, if the width d of the slit is fixed, the transmission cross section exhibits maxima when the above Fabry–Pérot resonance condition is satisfied by tuning the slit length h .

Figure 2(b) shows the transmission cross section σ_T of the plasmonic coaxial waveguide for the single-slit coupler as a function of the slit length h . We calculate the transmission cross section σ_T using FDTD. The peaks in the transmission cross section are associated with the slit Fabry–Pérot resonances. The maximum transmission cross section corresponds to the first peak. This peak corresponds to the first slit Fabry–Pérot resonance. Also shown in

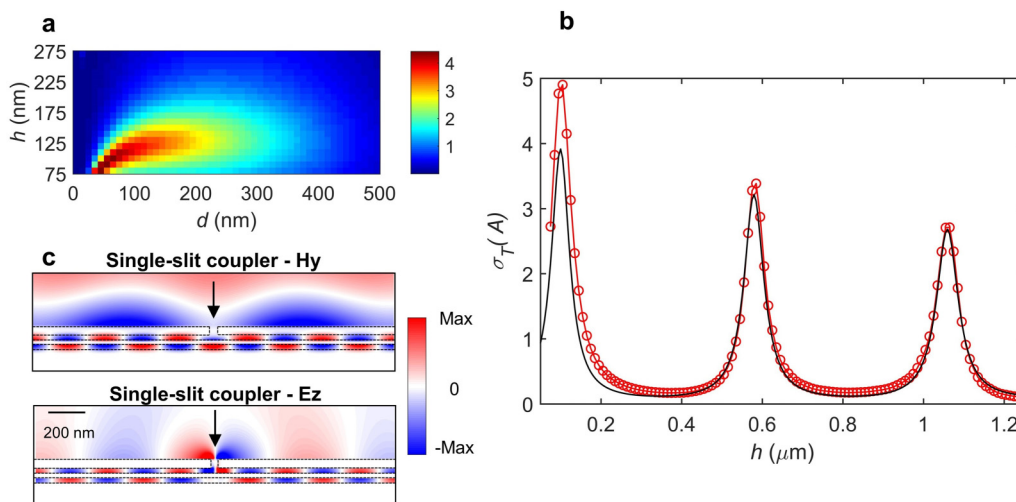


FIG. 2. (a) Transmission cross section σ_T of the plasmonic coaxial waveguide in units of A for the single-slit coupler structure of Fig. 1(a) as a function of the slit width d and length h [Fig. 1(b)] calculated using FDTD. Here, A is the area of the dielectric core in the cross section of the plasmonic coaxial waveguide [Fig. 1(d)]. Results are shown for $\lambda_0 = 1550 \text{ nm}$. All other parameters are as in Fig. 1(d). (b) Transmission cross section σ_T for the single-slit coupler structure of Fig. 1(a) as a function of the slit length h calculated using FDTD (red circles) and scattering matrix theory (black solid line). Results are shown for $d = 70 \text{ nm}$. All other parameters are as in Fig. 2(a). (c) Profiles of magnetic and electric field components for the single-slit coupler structure of Fig. 1(a) depicted at $y = 0$ [Fig. 1(d)]. Results are shown for the optimized slit parameters $d = 70 \text{ nm}$, $h = 95 \text{ nm}$. All other parameters are as in Fig. 2(a).

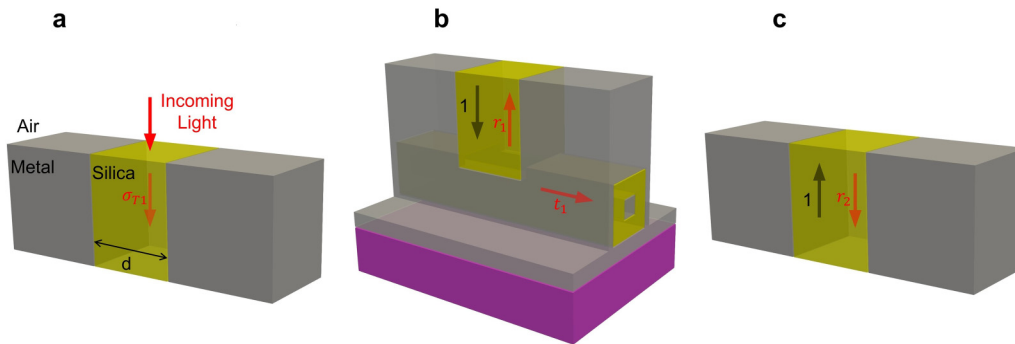


FIG. 3. Schematics defining different variables in the scattering matrix formalism. (a) The transmission cross section σ_{T_1} of the silver–silica–silver MDM slit for a normally incident plane wave. (b) The transmission and reflection coefficients, t_1 and r_1 , when the MDM slit mode is incident at the junction with the plasmonic coaxial waveguide. (c) The reflection coefficient r_2 at the slit/air interface.

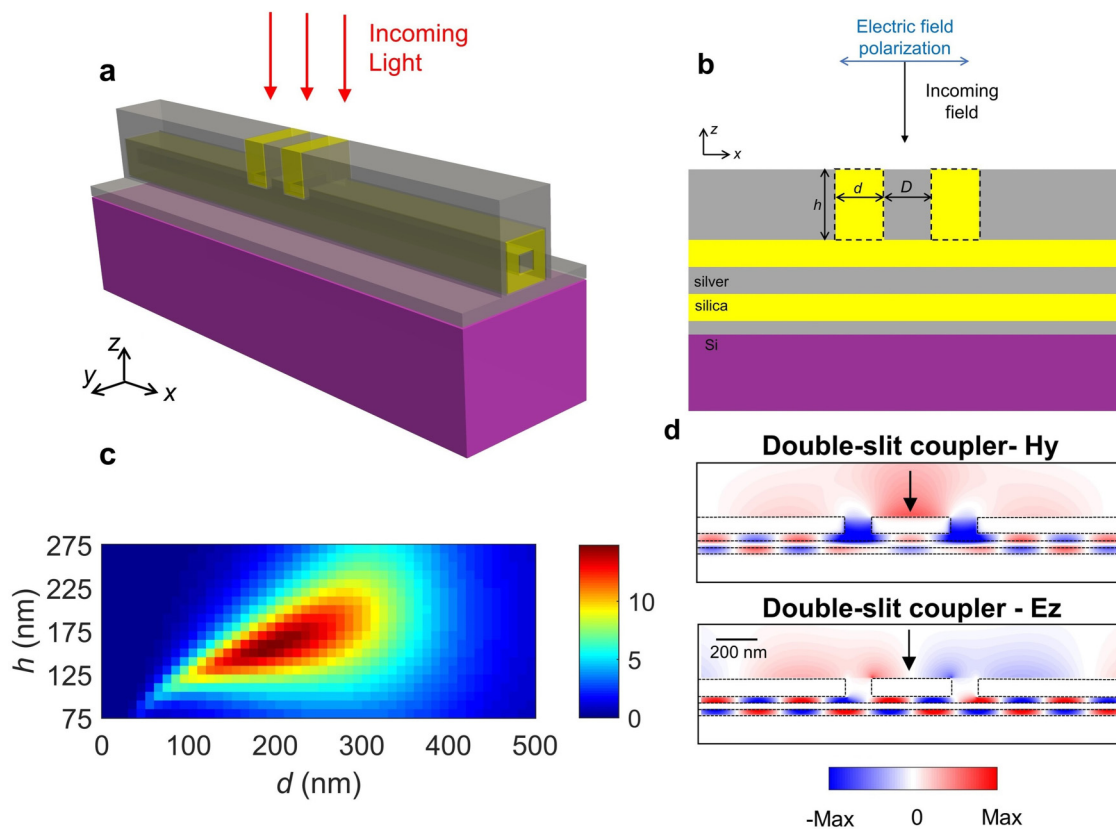


FIG. 4. (a) Schematic of the proposed double-slit nanostructure for exciting the fundamental guided mode of the plasmonic coaxial waveguide. The normally incident plane wave excites the guided modes of the slits that in turn excite the modes of the plasmonic coaxial waveguide. (b) Cross-sectional view of the coupler structure at the $y = 0$ plane. (c) Transmission cross section σ_T of the plasmonic coaxial waveguide in units of A for the double-slit coupler structure of Fig. 4(a) as a function of the slit width d and length h [Fig. 4(b)] calculated using FDTD. Here, A is the area of the dielectric core in the cross section of the plasmonic coaxial waveguide [Fig. 1(d)]. The total width of the incoupling structure is $2d + D = 1.1 \mu\text{m}$. Results are shown for $\lambda_0 = 1550 \text{ nm}$. All other parameters are as in Fig. 1(d). (d) Profiles of magnetic and electric field components for the double-slit coupler structure of Fig. 4(a). Results are shown for the optimized slit parameters $d = 210 \text{ nm}$, $h = 165 \text{ nm}$. All other parameters are as in Fig. 4(c).

the figure are the results of scattering matrix theory for calculating σ_T [Eq. (1)]. We find that the results of the scattering matrix theory agree very well with the exact results calculated with FDTD. However, for small slit lengths h , even though the resonance wavelength is correctly predicted by the theory, the predicted peak transmission cross section σ_T deviates from the numerical simulation result. This deviation is due to the fact that in the theory, direct coupling between free-space light and the fundamental mode of the plasmonic coaxial waveguide is not taken into account. For small slit lengths h , this direct coupling cannot be neglected.

For the optimized structure ($d = 70$ and $h = 95$ nm), the transmission cross section of the silver–silica–silver slit is $\sigma_{T_1} \simeq 5.02 A \simeq 1 \times 10^5 \text{ nm}^2$. The enhanced transmission cross section indicates that the plasmonic slit coupler collects incoming light from an effective area much larger than the geometrical area of the slit, which is $70 \times 200 \text{ nm} = 1.4 \times 10^4 \text{ nm}^2$. We also calculate the power transmission coefficient of the waveguide junction as $T_{\text{splitter}} \simeq 0.07$ and the resonance enhancement factor as $\eta_{\text{resi}} \simeq 11.10$ for the optimized single-slit structure. We observe

that the high resonance enhancement factor of the silver–silica–silver slit η_{resi} , compensates for the low power transmission coefficient of the waveguide junction, resulting in a high coupling efficiency to the fundamental mode of the plasmonic coaxial waveguide.

In Fig. 2(c), we show the profiles of the y component of the magnetic field H_y and the z component of the electric field E_z for the structure of Fig. 1(a) at $y = 0$ [Fig. 1(d)] for the optimized slit parameters $d = 70$ nm, $h = 95$ nm. We observe a large field enhancement in the plasmonic coaxial waveguide compared to the incident field because, as mentioned above, the plasmonic slit coupler collects light from an effective area much larger than the geometrical area of the slit.

B. Double-slit coupler

In order to further enhance the coupling efficiency from the free-space plane wave to the fundamental mode of the plasmonic coaxial waveguide, we investigate a double-slit structure [Fig. 4(a)]. We limit the width of the structure $2d + D$ to be less than $1.1 \mu\text{m}$

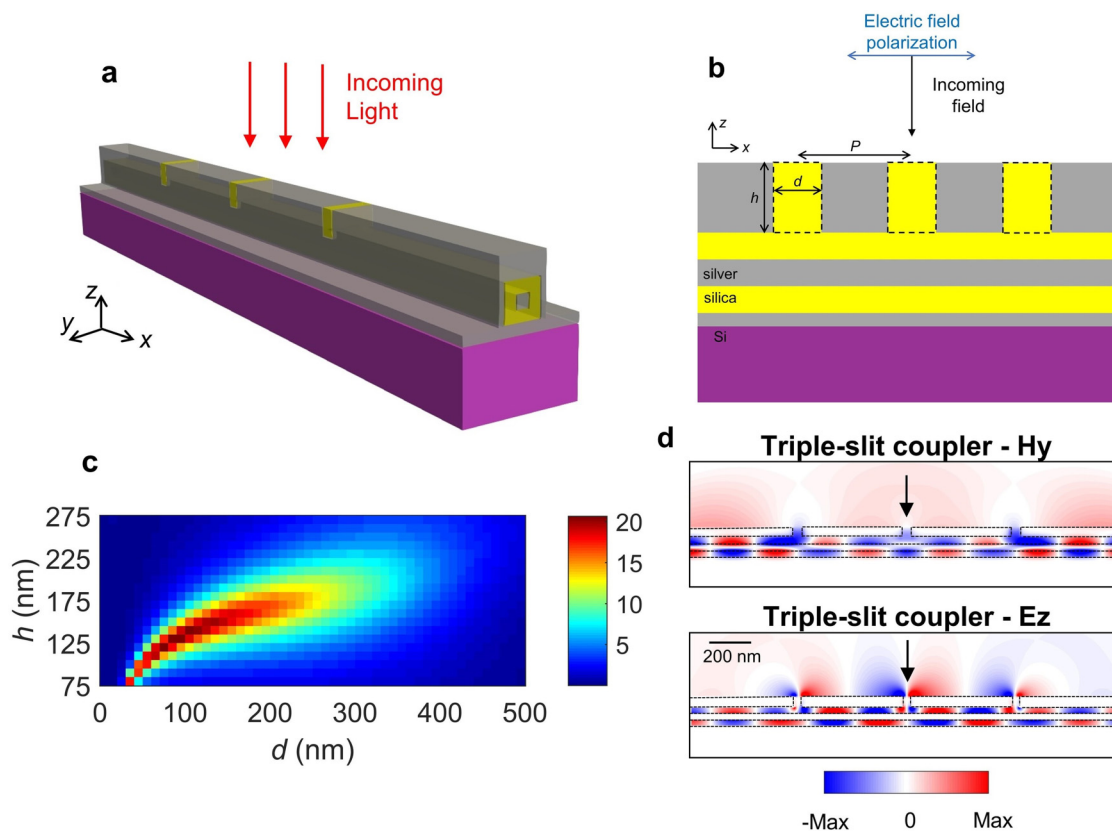


FIG. 5. (a) Schematic of the proposed triple-slit nanostructure for exciting the fundamental guided mode of the plasmonic coaxial waveguide. The normally incident plane wave excites the guided modes of the slits that in turn excite the modes of the plasmonic coaxial waveguide. (b) Cross-sectional view of the coupler structure at the $y = 0$ plane. (c) Transmission cross section σ_T of the plasmonic coaxial waveguide in units of A for the triple-slit coupler structure of Fig. 5(a) as a function of the slit width d and length h [Fig. 5(b)] calculated using FDTD. Here, A is the area of the dielectric core in the cross section of the plasmonic coaxial waveguide [Fig. 1(d)]. The distance between two adjacent slits is $P = 900$ nm. Results are shown for $\lambda_0 = 1550$ nm. All other parameters are as in Fig. 1(d). (d) Profiles of magnetic and electric field components for the structure of Fig. 5(a). Results are shown for the optimized slit parameters $d = 70$ nm, $h = 115$ nm. All other parameters are as in Fig. 5(c).

[Fig. 4(b)], which approximately corresponds to one wavelength of light in silica ($\lambda_s = \frac{\lambda_0}{n_s}$, where $n_s = 1.44$), when operating at the optical communication wavelength ($\lambda_0 = 1.55 \mu\text{m}$). In Fig. 4(c), we show the transmission cross section σ_T of the plasmonic coaxial waveguide for the structure of Figs. 4(a) and 4(b) as a function of the width d and length h of the slits calculated using FDTD. The maximum transmission cross section $\sigma_T \simeq 14.80 \text{ A}$ is obtained for $d = 210 \text{ nm}$ ($D = 680 \text{ nm}$) and $h = 160 \text{ nm}$. The maximum transmission cross section σ_T of the double-slit coupler is ~ 3.02 times larger than the one of the single-slit coupler. The greatly enhanced transmission cross section of the double-slit coupler is associated with the excitation of surface plasmons at the interface between the slits and air by the incident light waves. The surface plasmons are coupled into the slits and, therefore, lead to an increase in the transmission cross section of the structure.

In Fig. 4(d), we show the profiles of the y component of the magnetic field H_y and the z component of the electric field E_z for the structure of Fig. 4(a) at $y = 0$ [Fig. 1(d)] for the optimized slit parameters $d = 210 \text{ nm}$, $h = 165 \text{ nm}$. Similar to the single-slit coupler, we observe a large field enhancement in the plasmonic coaxial waveguide compared to the incident field because the structure collects light from an effective area much larger than its geometrical area.

C. Triple-slit coupler

In order to further enhance the coupling efficiency of the structure, we increase the number of slits and consider a triple-slit coupler. As we increase the number of resonators, we expect increased coupling efficiency from the free-space plane wave to the fundamental mode of the plasmonic coaxial waveguide. Here, we consider a symmetric triple-slit structure [Fig. 5(a)]. We vary the distance between adjacent slits P [Fig. 5(b)] and find that for $\lambda_0 = 1550 \text{ nm}$, the coupling efficiency is maximum for $P = 900 \text{ nm}$. Figure 5(c) shows the transmission cross section σ_T of the plasmonic coaxial waveguide in units of A for the structure of Fig. 5(a) as a function of the width d and length h of the slits calculated using FDTD. The maximum transmission cross section $\sigma_T \simeq 20.65 \text{ A}$ is obtained for $d = 70 \text{ nm}$ and $h = 115 \text{ nm}$. In the optimized triple-slit coupler, the transmission cross section of the plasmonic coaxial waveguide is ~ 4.21 and ~ 1.39 times larger than the one in the optimized single- and double-slit couplers, respectively. The number of incoupling slit resonators can be further increased. We found, however, that the transmission cross section σ_T does not significantly increase for structures with four or five slit resonators. On the other hand, the total size of the coupler greatly increases for four- and five-slit couplers. We, therefore, did not further consider couplers with more than three slits.

In Fig. 5(d), we show the profiles of the y component of the magnetic field H_y and the z component of the electric field E_z for the structure of Fig. 5(a) for the optimized slit parameters $d = 70 \text{ nm}$, $h = 115 \text{ nm}$. The triple-slit coupler has higher incoupling efficiency compared to the double-slit coupler. This, however, comes at the cost of a significantly larger size.

As discussed above, all incoupling structures were optimized at $\lambda_0 = 1.55 \mu\text{m}$. Even though the single-, double-, and triple-slit structures were optimized at a single wavelength, we observe that

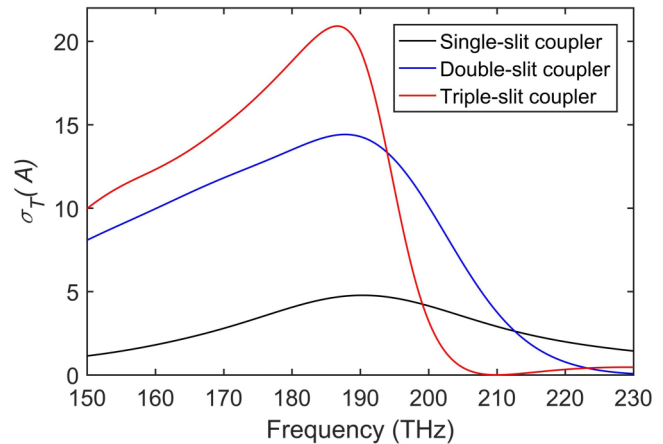


FIG. 6. Transmission cross sectional σ_T spectra in units of A for the optimized single-, double-, and triple-slit incoupling structures. Here, A is the area of the dielectric core in the cross section of the plasmonic coaxial waveguide [Fig. 1(d)]. Results are shown for the optimized structures of Figs. 2(c) (black line), 4(d) (blue line), and 5(d) (red line).

their transmission cross section is large in a broad wavelength range (Fig. 6). This indicates that the quality factors of these structures are low. Even though the transmission cross sections of the structures are enhanced, the enhancement does not originate from strong resonances.

D. Outcoupling structures

So far, we have investigated slit-based structures for incoupling free-space light into the fundamental mode of the plasmonic coaxial waveguide. It is also interesting to investigate light extraction from the plasmonic coaxial waveguide. In this subsection, we consider slit-based outcoupling structures for coupling the propagating mode of the plasmonic coaxial waveguide to free-space radiation that can be collected at a detector. We note that light extraction from plasmonic coaxial waveguides and the radiation pattern of such slit nanoantennas have not been investigated before.

Figure 7(a) shows the cross-sectional view of an outcoupling structure based on slit resonators. Here, we consider a triple-slit outcoupling structure. Single- and double-slit structures can also be used for outcoupling. As shown in the schematic, the fundamental mode of the plasmonic coaxial waveguide is incident from the left, and the slits act as nanoantennas that outcouple the propagating waveguide mode to free-space radiation. Here, θ is the angle between the direction of the maximum radiation intensity (main-lobe) and the z direction. In Fig. 7(b), we show the calculated local electric field amplitude immediately above the slits of the optimized triple-slit structure [Fig. 5(d)] when the fundamental mode of the waveguide at $\lambda_0 = 1550 \text{ nm}$ is incident from the left. We calculate the far-field radiation pattern of these slit nanoantennas using their calculated near-field distribution.⁴⁹ Figures 7(c)–7(e) show the far-field radiation pattern of the outcoupling structures with single-, double-, and triple-slit nanoantennas, respectively. We observe that,

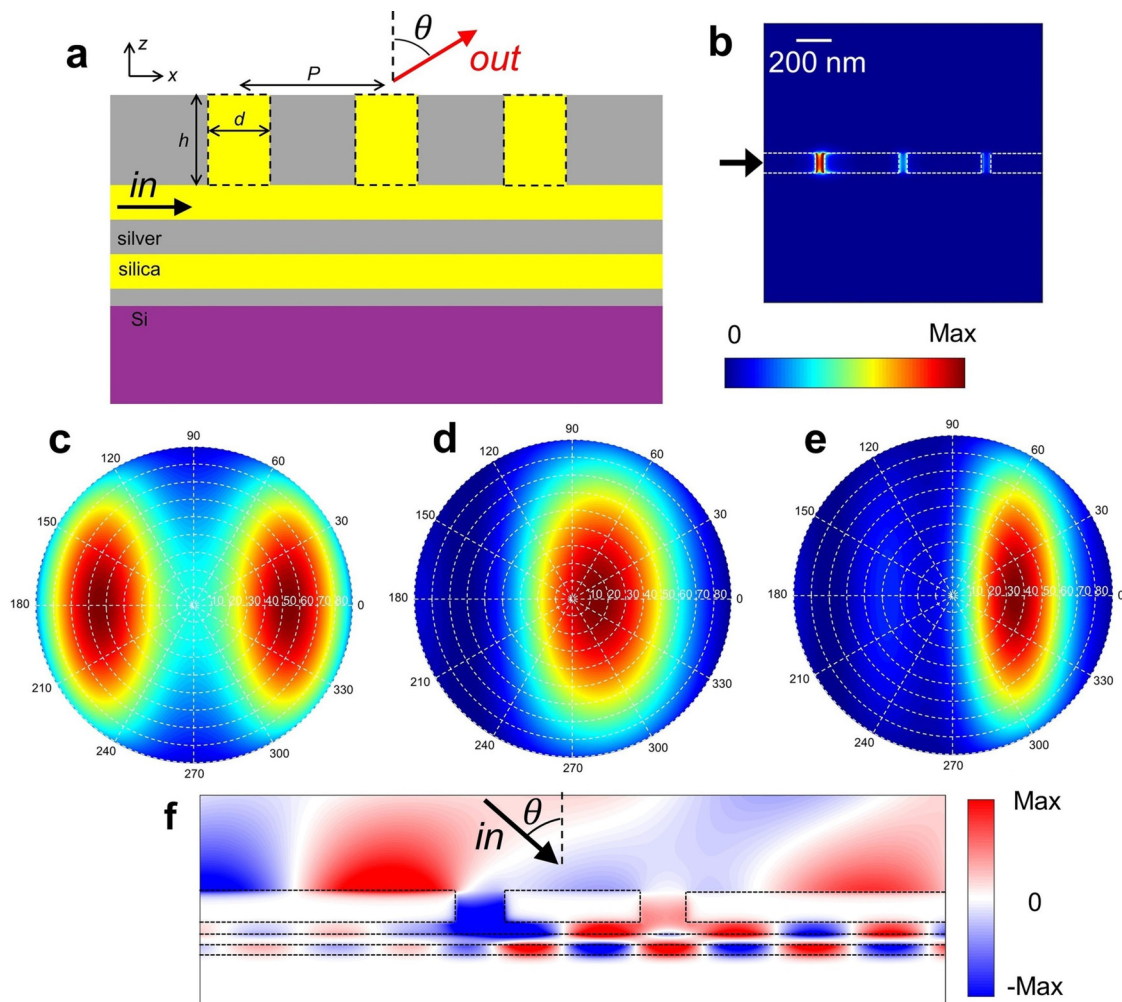


FIG. 7. (a) Schematic of a triple-slit coupler structure in a cross-sectional view at the $y = 0$ plane when the fundamental quasi-TEM mode of the plasmonic coaxial waveguide is incident from the left and the slits outcouple light to the free space. Here, θ is the angle between the direction of maximum radiation intensity (mainlobe) and the z direction. (b) Profile of the electric field amplitude calculated immediately above the interface between the slits and air [Fig. 7(a)]. All parameters are as in Fig. 5(d). (c) Far-field radiation pattern above the slit for the optimized single-slit structure when the fundamental quasi-TEM mode of the plasmonic coaxial waveguide is excited as in Fig. 7(a). Results are shown for the structure of Fig. 2(c). (d) Far-field radiation pattern above the slits for the optimized double-slit structure when the fundamental quasi-TEM mode of the plasmonic coaxial waveguide is excited as in Fig. 7(a). Results are shown for the structure of Fig. 4(d). (e) Far-field radiation pattern above the slits for the optimized triple-slit structure when the fundamental quasi-TEM mode of the plasmonic coaxial waveguide is excited as in Fig. 7(a). Results are shown for the structure of Fig. 5(d). (f) Profile of the magnetic field component H_y at the $y = 0$ plane when a plane wave is incident at an angle $\theta = 20^\circ$ on the optimized double-slit structure of Fig. 4(d). FDTD calculations show that $\sim 93.9\%$ of the power coupled into the waveguide couples to the right-propagating mode.

while the radiation pattern of the single-slit nanoantenna is symmetric, the radiation patterns of the double- and triple-slit structures are asymmetric. This asymmetric radiation pattern is a result of the asymmetric excitation of the slit nanoantennas, which leads to stronger resonant fields in the slits closest to the excitation source [Fig. 7(b)]. However, we found that, if the slit nanoantennas are symmetrically excited with waveguide modes incident from both the left and right directions, the radiation pattern becomes symmetric. The direction of the maximum radiation intensity of the slit nanoantennas can be adjusted by tuning the distance

between the slits and their dimensions. For instance, in Figs. 7(d) and 7(e), the radiation intensity is maximized for $\theta \sim 20^\circ$ and $\theta \sim 35^\circ$, respectively.

The asymmetric radiation pattern of the multiple-slit structures when used for outcoupling suggests that, if we adjust the angle of incidence of the free-space plane wave, the fundamental mode of the plasmonic coaxial waveguide can be asymmetrically excited by such multiple-slit structures when used for incoupling. More specifically, with a proper choice of the dimensions of the slit couplers and the angle of incidence of the free-space plane wave,

one can excite only the right- or only the left-propagating mode of the plasmonic coaxial waveguide. Figure 7(f) shows the profile of the y component of the magnetic field H_y at the $y = 0$ plane when a plane wave is incident from the free space at an angle $\theta = 20^\circ$ on the optimized double-slit structure of Fig. 4(a). Based on our FDTD calculations, $\sim 93.9\%$ of the power coupled into the waveguide couples to the right-propagating mode. We note that highly asymmetrical excitation of plasmonic waveguide modes typically requires nanostructures with multiple grooves or slits.⁵³ In contrast, in our structure, the highly asymmetrical excitation of the fundamental mode of the plasmonic coaxial waveguide is achieved with only two slits.

E. Switches for plasmonic coaxial waveguides

As discussed in Sec. I, coupling optical power into plasmonic waveguides is of paramount importance for applications of plasmonics. Another challenge for on-chip applications of plasmonics is developing active plasmonic devices such as switches and modulators.^{47,48} It is known that slowing down light in plasmonic waveguides leads to enhanced light-matter interaction and can, therefore, enhance the sensitivity to refractive index variations. The slow-light enhancement of the sensitivity in turn leads to enhanced switching and sensing performance.⁵⁴ Here, we use this concept to design compact switches for plasmonic coaxial waveguides.

Figure 8(a) shows the schematic of the proposed plasmonic coaxial waveguide-cavity structure investigated in this section. The

structure is built by side-coupling a periodic array of two stub resonators, consisting of plasmonic coaxial waveguides of finite length, to a plasmonic coaxial waveguide. This structure is based on a plasmonic analog of electromagnetically induced transparency and supports a slow-light mode.^{32,55} The structure exhibits plasmon-induced transparency through destructive interference of the two bright resonators in each period.⁵⁶ Figure 8(b) shows the top view schematic at $z = 0$ [Fig. 1(d)] of the proposed plasmonic coaxial waveguide-cavity structure. As before, the metal used is silver, and the space between the metallic parts is filled with an active material with a tunable refractive index. The active material used here is silicon dioxide doped with CdSe quantum dots with refractive index $n = 2.02 + i\kappa$.^{57,58} The imaginary part of the refractive index κ is tunable. The inner and outer metals at the end of the stubs are not connected [Fig. 8(a)] so that the stubs are open-circuited. We use open-circuited coaxial stub resonators because they lead to much more compact waveguide-cavity devices compared to short-circuited resonators.³² We calculate the transmission of the structures by normalizing their output power by the output power from a plasmonic coaxial waveguide of the same length without stubs. The stub lengths $d_1 = 25$ nm and $d_2 = 65$ nm [Fig. 8(b)] are chosen so that the transmission peak for $\kappa = 0$ is at $\lambda_0 = 1550$ nm. Figure 8(c) shows the transmission spectra for the structure of Fig. 8(a) for $\kappa = 0$ (transparent state of the active material) and $\kappa = 0.05$ (absorbing state of the material). The transparent state of the active material corresponds to the *on* state of the switch [Fig. 8(c)]. When κ changes to $\kappa = 0.05$ in the

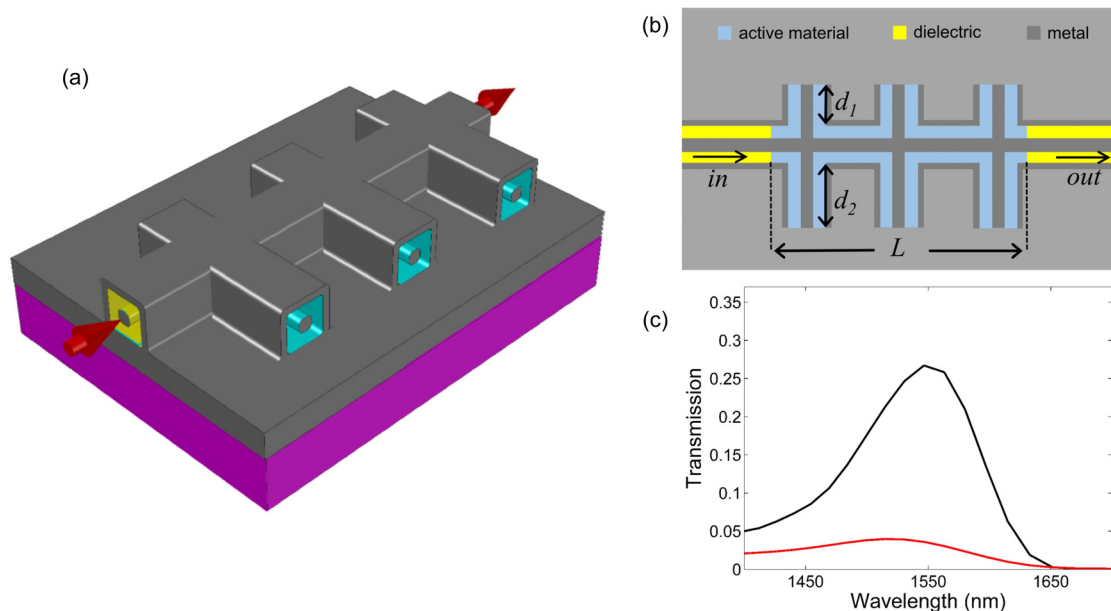


FIG. 8. (a) Schematic of a plasmonic coaxial waveguide side-coupled to a periodic array of two open-circuited coaxial stub resonators. The propagation direction of light is indicated by red arrows. The metal used is silver, and the space between the metallic parts is filled with an active material with refractive index $n = 2.02 + i\kappa$, where κ is tunable. (b) Top view schematic at $z = 0$ of the plasmonic coaxial waveguide side-coupled to the periodic array of two stub resonators. (c) Transmission spectra for the structure of Fig. 8(a) for $\kappa = 0$ (black) and $\kappa = 0.05$ (red). Results are shown for $d_1 = 25$ nm and $d_2 = 65$ nm. The length of the active region is $L = 1100$ nm. Three periods of the structure are included in the active region.

active region [Fig. 8(b)], the switch is turned *off* [Fig. 8(c)]. We find that the modulation depth of this structure, defined as the ratio of the transmission in the *on* state $T(\kappa = 0)$ to the transmission in the *off* state $T(\kappa = 0.05)$, is 8.7 dB at $\lambda_0 = 1550$ nm. Such a modulation depth is large enough for optical switching applications.

III. CONCLUSIONS

In this paper, we introduced wavelength-scale light coupling structures and switches for plasmonic coaxial waveguides. We started by investigating single-slit structures as couplers between free-space light and the fundamental mode of plasmonic coaxial waveguides. We found that, when the Fabry–Pérot resonance condition of the slit is satisfied, the transmission cross section is maximized. To further enhance the coupling into the plasmonic coaxial waveguide, we then investigated a double-slit structure. We found that the transmission cross section of the double-slit coupler is significantly larger than the one of the single-slit coupler. The greatly enhanced transmission cross section of the double-slit coupler is associated with the excitation of surface plasmons at the interface between the slits and air by the incident light waves. The surface plasmons are coupled into the slits and, therefore, lead to an increase in the transmission cross section of the structure. Overall, the double-slit coupler resulted in ~ 3.02 times enhancement of the coupling into the plasmonic coaxial waveguide compared to the single-slit coupler. To even further enhance the coupling into the plasmonic coaxial waveguide, we also considered a triple-slit structure. We found that, even though the coupling efficiency into the plasmonic coaxial waveguide for the optimized triple-slit structure increased ~ 1.39 times compared to the optimized double-slit structure, the size of the structure also significantly increased. We also found that, even though we optimized the single-, double-, and triple-slit structures at a single wavelength, their transmission cross section is large in a broad wavelength range.

In addition, we found that the same slit-based structures can couple the fundamental mode of the plasmonic coaxial waveguide to free-space radiation, enabling light extraction from the plasmonic coaxial waveguide. We observed that, while the far-field radiation pattern of a single-slit structure on top of the waveguide is symmetric, double- and triple-slit structures have asymmetric radiation patterns. This feature enables the tuning of the direction of maximum radiation of the slit nanoantennas. We also showed that the fundamental mode of the plasmonic coaxial waveguide can be asymmetrically excited by adjusting the angle of incidence of the free-space plane wave.

We finally designed compact plasmonic switches consisting of a plasmonic coaxial waveguide side-coupled to a periodic array of two open-circuited coaxial stub resonators. Such a structure is based on a plasmonic analog of electromagnetically induced transparency and supports a slow-light mode. The space between the metallic parts is filled with an active material with a tunable refractive index. The transparent (absorbing) state of the active material corresponds to the *on* (*off*) state of the switch. We found that the modulation depth of this structure is large enough for optical switching applications.

As final remarks, coaxial waveguides with square cross sections as in Fig. 1(d) can be fabricated using standard lithography-based methods.³¹ Thus, the proposed switches (Fig. 8) can be fabricated using lithography-based fabrication techniques.³¹ They could also be fabricated using metal-coated semiconductor nanowires.^{31,59} Since semiconductor nanowires can be grown into structures such as bends⁶⁰ and combs,⁶¹ they could be used to build networks of plasmonic coaxial waveguides³¹ as in Fig. 8. For the characterization of the proposed switches, incoupling and outcoupling slits (Subsections II A–II D) can be introduced to couple light into and out of the structures.^{43,46} Far-field illumination and detection techniques can then be used to characterize the structures.^{43,46}

ACKNOWLEDGMENTS

This research was supported by the National Science Foundation (NSF) (Award No. 1254934).

DATA AVAILABILITY

The data that support the findings of this study are available from the corresponding author upon reasonable request.

REFERENCES

- 1W. L. Barnes, A. Dereux, and T. W. Ebbesen, "Surface plasmon subwavelength optics," *Nature* **424**, 824–830 (2003).
- 2E. Ozbay, "Plasmonics: Merging photonics and electronics at nanoscale dimensions," *Science* **311**, 189–193 (2006).
- 3R. Zia, J. A. Schuller, A. Chandran, and M. L. Brongersma, "Plasmonics: The next chip-scale technology," *Mater. Today* **9**, 20–27 (2006).
- 4S. A. Maier and H. A. Atwater, "Plasmonics: Localization and guiding of electromagnetic energy in metal/dielectric structures," *J. Appl. Phys.* **98**, 011101 (2005).
- 5J. A. Schuller, E. S. Barnard, W. Cai, Y. C. Jun, J. S. White, and M. L. Brongersma, "Plasmonics for extreme light concentration and manipulation," *Nat. Mater.* **9**, 193–204 (2010).
- 6D. K. Gramotnev and S. I. Bozhevolnyi, "Plasmonics beyond the diffraction limit," *Nat. Photonics* **4**, 83–91 (2010).
- 7Z. Han and S. I. Bozhevolnyi, "Radiation guiding with surface plasmon polaritons," *Rep. Prog. Phys.* **76**, 016402 (2013).
- 8J. A. Dionne, L. A. Sweatlock, M. T. Sheldon, A. P. Alivisatos, and H. A. Atwater, "Silicon-based plasmonics for on-chip photonics," *IEEE J. Sel. Top. Quantum Electron.* **16**, 295–306 (2010).
- 9J. Takahara, S. Yamagishi, H. Taki, A. Morimoto, and T. Kobayashi, "Guiding of a one-dimensional optical beam with nanometer diameter," *Opt. Lett.* **22**, 475–477 (1997).
- 10Y. Bian and Q. Gong, "Deep-subwavelength light routing in nanowire-loaded surface plasmon polariton waveguides: An alternative to the hybrid guiding scheme," *J. Phys. D: Appl. Phys.* **46**, 445105 (2013).
- 11S. I. Bozhevolnyi, V. S. Volkov, E. Devaux, J. Y. Laluet, and T. W. Ebbesen, "Channel plasmon subwavelength waveguide components including interferometers and ring resonators," *Nature* **440**, 508–511 (2006).
- 12D. F. P. Pile and D. K. Gramotnev, "Plasmonic subwavelength waveguides: Next to zero losses at sharp bends," *Opt. Lett.* **30**, 1186–1188 (2005).
- 13Y. Zhu, X. Hu, H. Yang, and Q. Gong, "On-chip plasmon-induced transparency based on plasmonic coupled nanocavities," *Sci. Rep.* **4**, 3752 (2014).
- 14S. Zhu, T. Y. Liow, G. Q. Lo, and D. L. Kwong, "Fully complementary metal-oxide-semiconductor compatible nanoplasmonic slot waveguides for silicon electronic photonic integrated circuits," *Appl. Phys. Lett.* **98**, 021107 (2011).

- ¹⁵Y. Bian and Q. Gong, "Metallic-nanowire-loaded silicon-on-insulator structures: A route to low-loss plasmon waveguiding on the nanoscale," *Nanoscale* **7**, 4415–4422 (2015).
- ¹⁶R. F. Oulton, V. J. Sorger, D. A. Genov, D. F. P. Pile, and X. Zhang, "A hybrid plasmonic waveguide for subwavelength confinement and long-range propagation," *Nat. Photonics* **2**, 496–500 (2008).
- ¹⁷Y. Bian and Q. Gong, "Deep-subwavelength light confinement and transport in hybrid dielectric-loaded metal wedges," *Laser Photonics Rev.* **8**, 549–561 (2014).
- ¹⁸J. R. Krenn, B. Lamprecht, H. Ditlbacher, G. Schider, M. Salerno, A. Leitner, and F. R. Aussenegg, "Non diffraction-limited light transport by gold nanowires," *Europhys. Lett.* **60**, 663–669 (2002).
- ¹⁹S. A. Maier, P. G. Kik, H. A. Atwater, S. Meltzer, E. Harel, B. E. Koel, and A. A. G. Requicha, "Local detection of electromagnetic energy transport below the diffraction limit in metal nanoparticle plasmon waveguides," *Nat. Mater.* **2**, 229–232 (2003).
- ²⁰R. Zia, M. D. Selker, P. B. Catrysse, and M. L. Brongersma, "Geometries and materials for subwavelength surface plasmon modes," *J. Opt. Soc. Am. A* **21**, 2442–2446 (2004).
- ²¹G. Veronis and S. Fan, "Bends and splitters in subwavelength metal-dielectric-metal plasmonic waveguides," *Appl. Phys. Lett.* **87**, 131102 (2005).
- ²²A. Hosseini and Y. Massoud, "Nanoscale surface plasmon based resonator using rectangular geometry," *Appl. Phys. Lett.* **90**, 181102 (2007).
- ²³Y. Matsuzaki, T. Okamoto, M. Haraguchi, M. Fukui, and M. Nakagaki, "Characteristics of gap plasmon waveguide with stub structures," *Opt. Express* **16**, 16314–16325 (2008).
- ²⁴X. S. Lin and X. G. Huang, "Tooth-shaped plasmonic waveguide filters with nanometer sizes," *Opt. Lett.* **33**, 2874–2876 (2008).
- ²⁵C. Min and G. Veronis, "All-optical absorption switches in subwavelength metal-dielectric-metal plasmonic waveguides," *Proc. SPIE* **7394**, 73941Y (2009).
- ²⁶D. M. Pozar, "A modern course in microwave engineering," *IEEE Trans. Educ.* **33**, 129–134 (1990).
- ²⁷E. N. Economou, "Surface plasmons in thin films," *Phys. Rev.* **182**, 539–554 (1969).
- ²⁸A. Mahigir, P. Dastmalchi, G. Veronis, W. Shin, P. B. Catrysse, M. L. Brongersma, S. Fan, and W. Cai, "Subwavelength plasmonic two-conductor waveguides," in *Wiley Encyclopedia of Electrical and Electronics Engineering*, edited by J. Webster (John Wiley & Sons, Inc., 2016).
- ²⁹R. de Waele, S. P. Burgos, A. Polman, and H. A. Atwater, "Plasmon dispersion in coaxial waveguides from single-cavity optical transmission measurements," *Nano Lett.* **9**, 2832–2837 (2016).
- ³⁰M. Khajavikhan, A. Simic, M. Katz, J. H. Lee, B. Slutsky, A. Mizrahi, V. Lomakin, and Y. Fainman, "Thresholdless nanoscale coaxial lasers," *Nature* **482**, 204–207 (2012).
- ³¹W. Shin, W. Cai, P. B. Catrysse, G. Veronis, M. L. Brongersma, and S. Fan, "Broadband sharp 90-degree bends and T-splitters in plasmonic coaxial waveguides," *Nano Lett.* **13**, 4753–4758 (2013).
- ³²A. Mahigir, P. Dastmalchi, W. Shin, S. H. Fan, and G. Veronis, "Plasmonic coaxial waveguide-cavity devices," *Opt. Express* **23**, 20549–20562 (2015).
- ³³D. Yoo, D. A. Mohr, F. Vidal-Codina, A. John-Herpin, M. Jo, S. Kim, J. Matson, J. D. Caldwell, H. Jeon, N.-C. Nguyen, L. Martin-Moreno, J. Peraire, H. Altug, and S.-H. Oh, "High-contrast infrared absorption spectroscopy via mass-produced coaxial zero-mode resonators with sub-10 nm gaps," *Nano Lett.* **18**, 1930–1936 (2018).
- ³⁴D. Yoo, K. L. Gurunatha, H.-K. Choi, D. A. Mohr, C. T. Ertsgaard, R. Gordon, and S.-H. Oh, "Low-power optical trapping of nanoparticles and proteins with resonant coaxial nanoaperture using 10 nm gap," *Nano Lett.* **18**, 3637–3642 (2018).
- ³⁵Y. M. Calm, L. D'Imperio, N. T. Nesbitt, J. M. Merlo, A. H. Rose, C. Yang, K. Kempa, M. J. Burns, and M. J. Naughton, "Optical confinement in the nanocoax: Coupling to the fundamental TEM-like mode," *Opt. Express* **28**, 32152–32164 (2020).
- ³⁶G. Veronis and S. Fan, "Theoretical investigation of compact couplers between dielectric slab waveguides and two-dimensional metal-dielectric-metal plasmonic waveguides," *Opt. Express* **15**, 1211–1221 (2007).
- ³⁷Y. Huang, C. J. Min, and G. Veronis, "Compact slit-based couplers for metal-dielectric-metal plasmonic waveguides," *Opt. Express* **20**, 22233–22244 (2012).
- ³⁸E. Feigenbaum and M. Orenstein, "Modeling of complementary (void) plasmon waveguiding," *J. Lightwave Technol.* **25**, 2547–2562 (2007).
- ³⁹R. A. Wahsheh, Z. L. Lu, and M. A. G. Abushagur, "Nanoplasmonic couplers and splitters," *Opt. Express* **17**, 19033–19040 (2009).
- ⁴⁰R. X. Yang, R. A. Wahsheh, Z. L. Lu, and M. A. G. Abushagur, "Efficient light coupling between dielectric slot waveguide and plasmonic slot waveguide," *Opt. Lett.* **35**, 649–651 (2010).
- ⁴¹J. Tian, S. Q. Yu, W. Yan, and M. Qiu, "Broadband high-efficiency surface-plasmon-polariton coupler with silicon-metal interface," *Appl. Phys. Lett.* **95**, 013504 (2009).
- ⁴²C. Delacour, S. Blaize, P. Grosse, J. M. Fedeli, A. Bruyant, R. Salas-Montiel, G. Lerondel, and A. Chelnokov, "Efficient directional coupling between silicon and copper plasmonic nanoslot waveguides: Toward metal-oxide-silicon nanophotonics," *Nano Lett.* **10**, 2922–2926 (2010).
- ⁴³J. A. Dionne, H. J. Lezec, and H. A. Atwater, "Highly confined photon transport in subwavelength metallic slot waveguides," *Nano Lett.* **6**, 1928–1932 (2006).
- ⁴⁴H. J. Lezec, J. A. Dionne, and H. A. Atwater, "Negative refraction at visible frequencies," *Science* **316**, 430–432 (2007).
- ⁴⁵P. Neutens, P. Van Dorpe, I. De Vlamincq, L. Lagae, and G. Borghs, "Electrical detection of confined gap plasmons in metal-insulator-metal waveguides," *Nat. Photonics* **3**, 283–286 (2009).
- ⁴⁶K. Diest, J. A. Dionne, M. Spain, and H. A. Atwater, "Tunable color filters based on metal-insulator-metal resonators," *Nano Lett.* **9**, 2579–2583 (2009).
- ⁴⁷W. Cai, J. S. White, and M. L. Brongersma, "Compact, high-speed and power-efficient electrooptic plasmonic modulators," *Nano Lett.* **9**, 4403–4411 (2009).
- ⁴⁸N. Kinsey, M. Ferrera, V. Shalae, and A. Boltasseva, "Examining nanophotonics for integrated hybrid systems: A review of plasmonic interconnects and modulators using traditional and alternative materials," *J. Opt. Soc. Am. B* **32**, 121–142 (2015).
- ⁴⁹A. Taflov and S. C. Hagness, *Computational Electrodynamics* (Artech House, 2005).
- ⁵⁰R. C. Weast, M. J. Astle, and W. H. Beyer, *CRC Handbook of Chemistry and Physics* (CRC Press, Boca Raton, FL, 1988), Vol. 69.
- ⁵¹E. D. Palik, *Handbook of Optical Constants of Solids* (Academic, 1985), Vol. 3.
- ⁵²J.-M. Jin, *The Finite Element Method in Electromagnetics* (John Wiley & Sons, 2015), p. 800.
- ⁵³A. Baron, E. Devaux, J.-C. Rodier, J.-P. Hugonin, E. Rousseau, C. Genet, T. W. Ebbesen, and P. Lalanne, "Compact antenna for efficient and unidirectional launching and decoupling of surface plasmons," *Nano Lett.* **11**, 4207–4212 (2011).
- ⁵⁴Y. Huang, C. J. Min, S. H. Tao, and G. Veronis, "Design of compact Mach-Zehnder interferometer-based slow-light-enhanced plasmonic waveguide sensors," *J. Lightwave Technol.* **34**, 2796–2803 (2016).
- ⁵⁵Y. Huang, C. Min, and G. Veronis, "Subwavelength slow-light waveguides based on a plasmonic analogue of electromagnetically induced transparency," *Appl. Phys. Lett.* **99**, 143117 (2011).
- ⁵⁶K. M. Dhriti, M. Islam, A. Bhattacharya, A. Ahmad, and G. Kumar, "Plasmon-induced transparency in an air-dielectric grooved parallel-plate terahertz waveguide," *J. Opt. Soc. Am. B* **38**, 1290–1296 (2021).
- ⁵⁷C. Min and G. Veronis, "Absorption switches in metal-dielectric-metal plasmonic waveguides," *Opt. Express* **17**, 10757–10766 (2009).
- ⁵⁸D. Pacifici, H. J. Lezec, and H. A. Atwater, "All-optical modulation by plasmonic excitation of CdSe quantum dots," *Nat. Photonics* **1**, 402–406 (2007).
- ⁵⁹Y. J. Fang, J. Sha, Z. L. Wang, Y. T. Wan, W. W. Xia, and Y. W. Wang, "Behind the change of the photoluminescence property of metal-coated ZnO nanowire arrays," *Appl. Phys. Lett.* **98**, 033103 (2011).
- ⁶⁰C. J. Barrelet, A. B. Greytak, and C. M. Lieber, "Nanowire photonic circuit elements," *Nano Lett.* **4**, 1981–1985 (2004).
- ⁶¹J. Yao, H. Yan, and C. M. Lieber, "A nanoscale combing technique for the large-scale assembly of highly aligned nanowires," *Nat. Nanotechnol.* **8**, 329–335 (2013).